Title
A HYBRID STREAMER CHAMBER FOR INTERMEDIATE ENERGY HEAVY ION PHYSICS

Author
Bibber, K. Van

Publication Date
1981-11-01

LBL-15105
Preprint

Lawrence Berkeley Laboratory
UNIVERSITY OF CALIFORNIA

Published in Nuclear Instruments and Methods,
Vol. 198, 1982, pp. 253-262

A HYBRID STREAMER CHAMBER FOR INTERMEDIATE ENERGY HEAVY ION PHYSICS

K. Van Bibber, B.G. Harvey, D.L. Hendrie,
J. Mahoney, M.J. Murphy, and W.W. Pang

November 1981

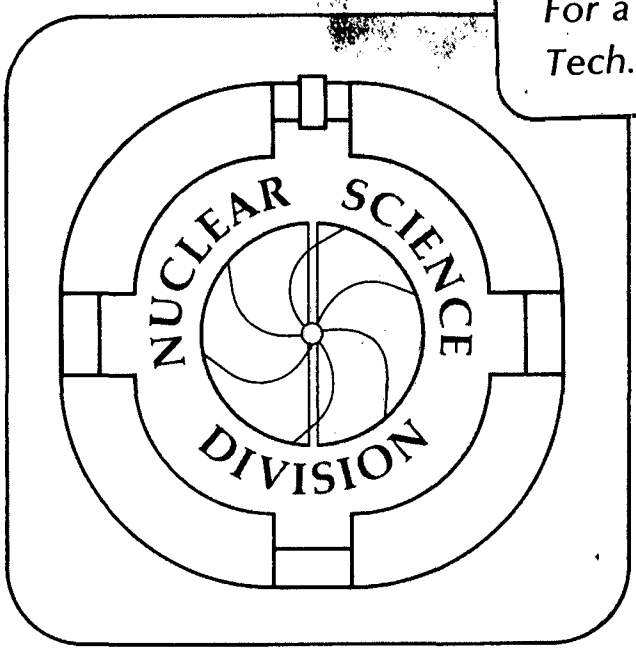

Prepared for the U.S. Department of Energy under Contract DE-AC03-76SF00098

DISCLAIMER

A HYBRID STREAMER CHAMBER FOR INTERMEDIATE ENERGY HEAVY ION PHYSICS*

K. Van Bibber

Department of Physics
Stanford University
Stanford, CA 94305

B. G. Harvey, D. L. Hendrie, J. Mahoney,
M. J. Murphy, W. W. Pang

Nuclear Science Division
Lawrence Berkeley Laboratory
University of California
Berkeley, CA 94720

ABSTRACT

A small volume streamer chamber currently in use at the Lawrence Berkeley Laboratory 88-inch cyclotron is described. A series of external solid state telescopes serves both as the event trigger, and to record the energy and particle identification of the leading fragment in the reaction.

The application of this device to the study of associated charged particle multiplicities in reactions of ^{16}O + CsI at 16.5 MeV/nucleon is presented to illustrate its capability.

---

*This work was supported by the Director, U.S. Office of Energy Research, Division of Nuclear Physics of the Office of High Energy and Nuclear Physics, and by Nuclear Sciences of the Basic Energy Sciences Program of the U.S. Department of Energy under Contract No. DE-AC03-76SF00098.

1. INTRODUCTION

Since its development almost twenty years ago,[1] the streamer chamber has found wide application in the field of elementary particle physics.[2] Nevertheless, in spite of such attractive features as triggerability and 4π optical sensitivity for arbitrarily high charged particle multiplicities, its use in nuclear science has been considerably more limited. Specialized chambers were employed in the search for double-β^- decay of ^{48}Ca,[3] and for the measurement of the p + ^4He analyzing power at 70 and 80 MeV.[4] During the past decade, the Bevalac 1.2 m streamer chamber has been used in studies of relativistic heavy ion collisions, as has the SKM 2 m chamber at the Dubna synchrophasotron, and the contributions of these chambers to high energy heavy ion work have recently been reviewed.[5,6]

The development of a small volume streamer chamber at the Lawrence Berkeley Laboratory 88-inch cyclotron represents the first application of this visual technique to low- and intermediate-energy heavy ion physics (bombarding energies up to 35 MeV/nucleon). In the course of its development to scientific productivity, a number of significant observations have been made: (1) even at 10-20 MeV/nucleon the multiplicities of charged particles associated with heavy ion reactions warrant the development of 4π detection capability, a sizeable fraction of events being kinematically incomplete in standard coincidence measurements; (2) with proper care in design, such chambers can be made sufficiently thin in energy loss to be feasible for reaction mechanism studies at energies as low as 10 MeV/nucleon; (3) in spite of the much greater primary ionization produced by charged particles at these low velocities (relative to the minimum ionization

or relativistic rise region) the image quality is extremely good, free of 'flares' and with adequate track definition to resolve trajectories separated by less than 1^{o}; (4) conventional solid state telescopes may be operated in close proximity to the chamber, permitting a wide variety of hybrid configurations; (5) although chambers designed for determination of magnetic rigidities should be a factor of two to three times larger in linear dimensions than the present design, the operation of small chambers is smooth and reliable; and (6) if the physics objectives are met with simple scanning rather than track measurement, the data analysis may be fairly rapid.

In section 2 the experimental configuration for the streamer chamber is presented, in section 3 operating experiences are discussed, and in section 4 its application to the measurement of associated charged particle multiplicities in the system ^{16}O + CsI at 16.5 MeV/nucleon is described to demonstrate its physics capability. Finally, the results of experimentation with volume gases other than Ne-He is described qualitatively in section 5, with a view to applications where gas targets are desired to observe very low energy recoils.

2. EXPERIMENTAL ARRANGEMENT

2.1. The Streamer Chamber

The present chamber is a single gap device of active volume (17.1 × 11.2 × 5.1 cm^3) and of lucite construction. Figure 1 shows the chamber with the target ladder removed and replaced by a fourth lateral port of 0.0025 cm mylar for beam-gas studies. The anode plane at the bottom of the chamber

is copper sheet; the cathode is 97% optically transmissive nickel mesh to permit photography parallel to the electric and magnetic fields. Both electrodes are separated from the volume gas by lucite to prevent a direct spark channel from being formed across the gap. The chamber is vacuum tight so that the gas pressure may be varied between 0 and 760 torr.

The pulsed high voltage is supplied to the anode by a three-stage Marx generator (Figure 2) of 16,800 nF per stage, all three stages of which are triggered. The intrinsically good rise time of the leading edge ($\approx$ 12 ns) is matched on the falling edge by pulse shaping with a pressurized coaxial spark gap immediately before the chamber. The output voltage of the Marx generator is typically chosen to be 50-75 kV.

The chamber lies horizontally on the lower pole tip of a "C" magnet, whose maximum field with an 18 cm gap is 11 kG at a current of 570A. The chamber is seen in top view in Figure 3a, and from the upstream direction in Figure 3b. Note that the camera views the gas volume along the direction of the electric field. This is accomplished by means of two diagonal mirrors, whereas the light-emitting diode (LED) display for the frame index may be kept apart from the region of high electromagnetic noise (due to the Marx generator) by positioning it directly above the camera.

The single Flight Research camera carries a cannister of 500' (4000 frames)of KO-2498 ASA 300 35 mm film. With a 90 mm macro lens, the demagnification of the system is 6. For the tests with various gases to be described in section 5, the mirrors were adjusted to include views of the chamber both parallel and perpendicular to the applied electric field,

after the target ladder flange on the beam right side of the chamber was removed in favor of a transparent port.

Due to the extent of the unclamped magnetic field resulting from the wide pole gap, the beam trajectory is significantly perturbed upstream of the chamber. To compensate for the bending and translation of the beam, a sliding seal radial offset was inserted before the last section of beam line and the beam is normally steered approximately two centimeters to the right. The last section of beam line, made of lucite to avoid sparking in the proximity of the streamer chamber, is mounted on the radial offset by means of a bellows so that a small angle may be introduced, and the line may follow the beam trajectory without interception. Prior to entry into the chamber volume, the beam must traverse a 0.0025 cm mylar window, a 7.5 cm air gap, and another mylar window. Upon exiting the chamber, the beam particles are counted in a plastic scintillator-photomultiplier detector.

A standard gas handling system flows commercial spark chamber mixture (90% Ne - 10% He) through the chamber, and is then vented to the atmosphere by a roughing pump. Purification or drying of the gas is unnecessary. A perspective photograph of the chamber configured for studies utilizing the chamber gas as a nuclear target is shown in Fig. 4.

2.2 Hybrid Trigger and Electronics

The chamber is triggered by the detection of a forward going charged particle in any one of three silicon ΔE-E telescopes. These detectors are mounted in an aluminum box in the magnet pole gap, just outside the chamber's downstream window. The entrance window to the detector box is made of

1.5 mg/cm^2 aluminum foil to complete the electrical shielding of the detectors. The silicon detectors and their preamplifiers are unaffected by magnetic fields of several kG; only the Berkeley tailpulse choppers for energy calibration need to be removed to a field-free region. However, it has been found to be impossible to adequately shield the detectors from the RF noise from the Marx generator pulse. Consequently, it is necessary to use a shaping time in the linear amplification circuit that is less than the elapsed time between the event and the HV pulse, in order to have a fully resolved linear signal before the arrival of the noise pulse. The ionization memory time of the chamber requires that the high voltage be applied within 1μs of the trigger event. We have found that a 0.4 μs linear shaping time adequately resolves the detector signal from the noise pulse for a trigger delay of 600 ns, while enabling reasonable charge resolution up to at least oxygen from Si(Li) detectors. Figure 5 summarizes the timing sequence for the trigger electronics.

Due to the requirement of a short trigger delay, it is not possible to inspect the amplitudes of the linear signals or an analogue particle identification as a condition for event trigger. However, the requirement of a fast coincidence between the ΔE and E detectors is completely satisfactory in rejecting all but a few unwanted events. After an event trigger is initiated by such a fast coincidence, a veto is applied for approximately 750 ms to prevent any new signals from triggering the chamber while the Marx generator recharges and the film is being indexed by the digital display.

Two methods of correlating the particle telescope information and the visual track recording have been sucessfully employed in experiments. In the first (Fig. 6a), an analogue particle identification is made and its output is presented in parallel to a chain of single-channel analyzers (SCA), each gating on a particular isotope or element. The SCA outputs are then fanned into an encoder, and thence to an LED display which directly incorporates the particle identification information in the photographic frame. However, the total energy of the leading fragment is lost.

In the second scheme (Fig. 6b), the linear signals are routed to an analogue-to-digital converter, accompanied by an incrementing event number, and written into a computer buffer and magnetic tape. The same event number indexes the photograph via the LED array; that the numbers are in fact identical is guaranteed by a comparator circuit which stops the run and signals an alarm if synchronization is lost. In this mode, windows on particle energy may be imposed at any later time in the data analysis.

In order to minimize interference from pulsed high voltage noise, it is important to locate the digital electronics in the counting area, leaving only the physical LED array in the chamber area.

3. SYSTEM PERFORMANCE

The performance of the chamber in tests with β^- -particles is in qualitative accord with other chambers. In Ne-He at one atmosphere, for example, a streamer density of approximately 2.5 cm^{-1} is observed. The response to heavy ions is remarkably constant over a wide range of gas

pressure and voltage, as expected for operation in the streamer regime where space charge effects largely dominate streamer density. Normally the chamber is operated at a pressure of only 400 torr to minimize energy loss of the beam and secondary particles in the gas as well as to reduce the number of interactions with gas nuclei. The use of much lower pressures is prohibited by the effects of electron diffusion upon the track clarity.

Acceptable light output is obtained even at rather low electric field strengths (8-12 kV/cm), and individual streamers are discerned with a diameter of $\approx$ 1 mm viewed end-on. As is seen in Fig. 7, which shows the collision of ^{12}C + Ne at 35 MeV/nucleon, the image is typically flare-free. A major factor in the elimination of flares, which have plagued most chambers in use for data production, is almost certainly the use of low electric fields. Also evident in Fig. 7 is the insensitivity of track density to primary ionization. (Compare the beam track to those of the secondaries which, on the basis of their large number with respect to the total charge of the composite system, must consist mostly of particles of ^{4}He or lighter.)

Streamers in the present chamber are observed to grow nearly across the full extent of the gap, due to the moderately wide high voltage pulse ($\approx$ 25 ns FWHM) (see Fig. 8). Strictly speaking, chambers in which the streamers grow too long to directly show the depth dimension should be termed track projection chambers, but even in that case the dip angle of a track can be inferred from the track end point on the chamber wall, if one knows the location of the beam spot on target sufficiently well.

The stability of the high voltage waveform is good, judging from the oscilloscope photograph in Fig. 8, which is a record of 250 consecutive firings of the Marx generator, monitored at the streamer chamber. What is not evident in Fig. 8, for which an internal oscilloscope trigger was used , is a slight variation in time between the Marx trigger and the high voltage pulse due to statistical fluctuations in spark breakdown between the stages of the Marx generator. This fluctuation is small with respect to the total trigger delay time, and consequently is of no importance. A maximum event rate of one event per 0.75 second was chosen somewhat arbitrarily to protect the components of the Marx generator from premature failure due to rapid firing. (Operation at low electric fields also minimizes the periodic maintenance necessary for the Marx generator.) In practice, the average trigger rate was usually lower due to a limitation on the maximum beam intensity consistent with having predominently only one beam track in each photograph.

The picture quality deteriorates continuously with increasing delay time between the event and the high voltage pulse, with the tracks becoming diffuse and discontinuous, and drifting across the chamber. A qualitative estimate of the maximum delay before the picture is not able to be reliably scanned is 2 μs, even with pure Ne-He gas. This very short intrinsic memory time , when compared with the much longer times for pure gas in large chambers (typically 50 μs or more), suggests that the chamber may be self-quenching, due to outgassing from the chamber itself and its large surface-to-volume ratio. Although in principle the maximum tolerable beam rate should be $\approx 5 \times 10^5$ sec^{-1}, in fact old beam tracks are still visible with an

order of magnitude less beam, although they do not normally interfere with the scanning of a real event.

As the camera is shutterless and the film may remain exposed on the platens for as long as 30 seconds between events, care must be taken to totally darken the area surrounding the streamer chamber; this is accomplished by surrounding the magnetic volume with a black shroud, and making the target cave itself light tight.

The particle identification in the Si(Li) telescopes for heavy ions up to at least oxygen has proven satisfactory, despite the short linear shaping time and the distribution of entry angles into the telescopes due to (i) events occuring in the chamber gas and windows, (ii) the differences in radii of curvature of secondaries, and (iii) multiple scattering. A typical particle identification spectrum for ^{16}O induced reactions is shown in Fig. 9; this spectrum was produced by off-line software particle identification (scheme of Fig. 6b).

4. APPLICATION TO HEAVY ION TRANSFER AND FRAGMENTATION PROCESSES AT E/A $\lesssim$ 20 MeV/N

It has been suggested that the changes in production cross sections and in quasi-elastic fragment momentum widths that are observed in the vicinity of 15-20 MeV/A might be due to the role of a limiting angular momentum for transfer reactions.[7] At lower beam velocities, transfer or incomplete fusion reactions occur, and lead to two-body final states (when subsequent evaporation is ignored). At higher velocities transfer can no longer happen and the dominant mechanism becomes projectile fragmentation into two or more particles ($\geq$ three-body

final states). It has furthermore been predicted that the transfer and fragmentation components in the production of a particular ejectile should have characteristically different energy spectra.[7]

The hybrid streamer chamber is an ideal detector to study these aspects of heavy ion reactions, due to its ability to record all charged particles escaping the target following the reaction. Although in principle the relative contributions of two-body transfer and projectile breakup mechanisms to the production of a particular ejectile could be measured by a heavy ion-light ion coincidence experiment, this has never been achieved due to the requirements of accurate normalization, exhaustive out-of-plane as well as in-plane measurements, and the necessity of multiple light ion telescopes each designed for a different dynamic range of energy and mass of the anticipated light ion partner. Moreover, it is well known that coincidence experiments employing conventional, small-solid-angle detectors introduce strong kinematical biases. The streamer chamber suffers no such biases.

Motivated by these questions pertaining to transfer versus fragmentation mechanisms, an experiment using this hybrid chamber to observe ^{16}O + CsI reactions at 16.5 MeV/nucleon has been conducted at the LBL 88-inch cyclotron. The reaction energy represents the degradation in the extracted beam energy of 315 MeV upon entering the streamer chamber and reaching the middle of the 49 mg/cm^2 target. (As in other streamer chambers, the targets normally must be non-conducting if placed inside the fiducial volume). In the initial run, some of whose results are presented here, the particle identification was performed in hardware,

and the energy information of the trigger particle was not preserved. (In a subsequent run, the telescope data were collected in the computer, and later merged with the scanning data, which was transferred to computer cards and tape.) Approximately 15,000 photographs were taken in the first run with two targets, some 55% of which represent valid beam-target interactions. Events were triggered by a single particle telescope situated at each of three forward angles bracketing the grazing angle. Figure 10 shows two typical events.

The associated multiplicity distributions as a function of ejectile Z and angle are displayed in Fig. 11. Note that the trigger particle itself is counted and thus all events have $M \geq 1$. The data were scanned for the total multiplicity of secondary charged particles, and subdivided into the multiplicity of secondaries in sectors of $\pm 45^{\circ}$ of the beam in projected angle, and backward of 90°. Although these data represent only a preliminary selection of the total data taken so far, they illustrate the capability of separating the inclusive telescope data into operationally defined categories. For example, the ratio of $M = 1$ events to $M > 1$ events for a given ejectile Z may be derived and compared directly to calculations of the transfer probability as a function of transferred mass. Similarly, the telescope data may be replayed from tape, selectively sorting energy spectra according to multiplicity, and the predictions of reference 7 examined. It is important to realize that reference to other experiments may be necessary to determine how significantly our inferences may need to be qualified due to the neglect of pre-equilibrium neutrons (to which the streamer chamber is insensitive).

It is appropriate to remark that operation of streamer chambers at low energies requires a compromise between two opposing considerations with regard to target thickness. Targets as thick as possible are desirable to improve the ratio of events occurring in the target to events occurring elsewhere in the beam path. On the other hand, the physics objective will normally dictate a maximum acceptable thickness on the basis of energy resolution. In the present case, the beam enters the target at 17.8 MeV/n and exits at 14.9 MeV/n. Surprisingly, however, Monte Carlo calculations of the observed spectra in the trigger telescopes based on energy loss and straggling folded with the intrinsic spectral widths demonstrate that in the present case, the correction to the observed widths is not large.

5. INVESTIGATION OF STREAMER FORMATION IN OTHER GASES

Applications of streamer chambers are anticipated where it will be of interest to observe even the lowest energy recoils, and where the energy loss in solid targets would be prohibitive. The optimal solution is to find gas targets which will also serve as useful volume gases in streamer chambers.

Streamer chambers filled with hydrogen and helium have been made to perform passably, but at much higher electric field strengths. A survey with our chamber of the heavier noble gases argon and xenon has been carried out as a function of electric field strength E and pressure P for both minimum-ionizing β^-. and for heavy ions.

In tests with β's, streamer formation is observed to occur for both Ar and Xe, but at significantly higher values of E/P than is necessary

for Ne-He mixtures. Tracks with pure Ar were diffuse and ill-defined (Fig. 12 (b)), and disappeared rapidly with increasing pressure. Small admixtures of methane above the 0.1% level, however, radically changed the performance of the chamber. Tracks were now defined by bright, narrow and well-localized streamers (Fig. 12 (c)) having a density of ≈ 1.5 cm^{-1}, or about a factor of two less than that observed in Ne-He. Figure 12 (d) and 12 (e) (3.5% and 1.75% methane) show streamers simultaneously photographed parallel and perpendicular to the electric field; the filamentary appearance of the streamers viewed from the side is qualitatively similar to that with neon. The regularity of the streamer spacing and pronounced spreading of the discharge transverse to the particle trajectory (and hence to the direction of neighboring streamers) suggest a space charge effect. The onset of streamers in pure xenon occurs at still higher values of E and lower P and with a correspondingly lower linear density. Perpendicular to the applied field (Fig. 12 (f)), streamers in pure xenon are characterized by bright spherical discharges with filaments emanating in both directions along the field.

In-beam studies with argon-methane mixtures at various fields and pressures yielded pictures of relatively poor quality. The two-body fragmentation of ^{12}C at 420 MeV shown in Fig. 13 is representative of the behaviour with heavy ions, whereas more lightly ionizing secondaries were frequently difficult to recognize due to the scarcity of streamers along the tracks. Similar tests with pure xenon were negative at these low fields. The obvious solution for the use of gas targets which by themselves perform only marginally as streamer gases, is to fill only a

restricted channel or volume along the beam path with the desired gas, and the rest of the chamber with Ne-He, the two subvolumes being separated by thin windows.

6. Conclusions

Our initial studies with a small volume hybrid streamer chamber indicate that such chambers may be useful tools in low and intermediate energy heavy ion physics for the study of multiparticle final states. The intrinsic performance of such a chamber itself is uncritical, and conventional silicon detectors and electronics can be used in conjunction with the streamer chamber to greatly augment the capability of either alone.

Operation at low electric field strengths (8 - 12 kV/cm) practically eliminates all flaring in the chamber. (A reduction in flaring at a large volume chamber has been observed with reduced field strengths, but at the expense of reduced light output and the necessity of adding image intensifiers to the cameras.[8]) In the present case, no such light multiplication is necessary, probably due to the higher primary ionization associated with non-relativistic charged particles.

At present, the magnetic rigidity p/q is not extracted from the tracks of secondaries because the tracks are too short and distortion is noticeable, particularly near the walls of the chamber due to electrostatic buildup on the lucite. Momenta should be accessable in chambers roughly 50 cm in length, either with the addition of another view for stereoscopic reconstruction (necessitating another camera, or another mirror) or by observing

the track's exit point from the chamber, possibly by incorporating scintillators into the chamber construction and reading the array out event by event. Charge-coupled devices to eliminate film as an intermediary appear promising for larger chambers, but the costs associated with their implementation are significant.

We acknowledge the efforts of D. K. Scott, M. Avery and E. Bloemhof in the early phases of the project. We thank the entire crew of the 88-inch cyclotron for their efforts in extracting the high quality, low intensity heavy ion beams required for our operation.

This work was supported by the Director, U.S. Office of Energy Research, Division of Nuclear Physics of the Office of High Energy and Nuclear Physics, and by Nuclear Sciences of the Basic Energy Sciences Program of the U.S. Department of Energy under Contract No. DE-AC03-76SF00098.

REFERENCES

1. G. E. Chikovani, V. N. Roinishvili, V. A. Mikhailov, Phys. Lett. 6 254 (1963).
   G. E. Chikovani, V. N. Roinishvili, V. A. Mikhailov, Nucl. Inst. and Meth. 29 261 (1964).
   B. A. Dolgoschein, B. U. Rodionov, B. I. Luchkov, Nucl. Inst. and Meth. 29 270 (1964).
2. J. M. Watson, ed., Proceedings of the First International Conference on Streamer Chamber Technology, September 14-15, 1972, ANL-8055 (Instruments).
3. R. K. Bardin, P. J. Gollon, J. D. Ullman, C. S. Wu, Phys. Lett. 26B 112 (1967).
   J. D. Ullman, R. K. Bardin, P. J. Gollon, C. S. Wu, Nucl. Inst. and Meth. 66 1 (1968).
4. A. W. Stetz, V. Perez-Mendez, Nucl. Instr. and Meth. 73 34 (1969).
5. L. S. Schroeder, Nucl. Inst. and Meth. 162 395 (1979).
6. K. Van Bibber, A. Sandoval, "Streamer Chambers for Heavy Ions", in Heavy Ion Science, Vol. IV, (D. A. Bromley, ed.) Plenum Press, New York (to be published).
7. K. W. McVoy, M. C. Nemes, Z. Physik A295 177 (1980).
8. K. Wolf, private communication.

FIGURE CAPTIONS

Fig. 1. The 88-inch cyclotron streamer chamber.

Fig. 2. (a) Three-stage Marx generator. (b) Pulse shaping spark gap. The low inductance resistor dissipates the energy and prevents pulse reflections back into the Marx generator.

Fig. 3. (a) Top view of the hybrid streamer chamber. (b) Upstream view; pulse shaping spark gap and high voltage probe not shown.

Fig. 4. Perspective view of the streamer chamber for studies utilizing the chamber gas as a nuclear target. (a) Streamer chamber and diagonal mirror. (b) JUPITER C-magnet. (c) scintillator-phototube trigger detector. (d) beam pipe. (e) pulse shaping coaxial spark gap. (f) Marx generator. (g) high voltage probe. (h) camera. (i) diagonal mirror. (j) scintillator-phototube trigger detector. In the present hybrid configuration, scintillators (c) and (j) would be absent; target ladder, digital display, and telescope housing would be visible.

Fig. 5. Timing sequence for a single event cycle.

Fig. 6. Schematic of triggering schemes for hybrid operation. (a) Particle identification directly incorporated onto the film plane. (b) Event mode recording of telescope data along with event number. Fast and slow electronics denoted by "F" and "S", respectively.

Fig. 7. Interaction of ^{12}C + Ne at 35 MeV/nucleon. Beam enters from the left.

Fig. 8. High voltage pulse profile monitored at the chamber. Record consists of approximately 250 consecutive Marx firings.

Fig. 9. Particle identification spectrum produced by a downstream Si(Li) ΔE-E telescope, for the reactions of ^{16}O + CsI at 16.5 MeV/nucleon. The spectrum was recreated in software, according to the scheme of Fig. 6(b).

Fig. 10. Typical events for ^{16}O induced reactions with mylar. Beam enters from the right; mid-target energy is approximately 16.5 MeV/nucleon. Arrow to the left of each photograph indicates the trigger particle and its identity according to the gate number.

Fig. 11. Associated multiplicity distributions as a function of ejectile and angle for ^{16}O + CsI at 16.5 MeV/nucleon. (Preliminary data.)

Fig. 12. Tracks of ^{90}Sr β^- in the 88-inch cyclotron streamer chamber with various gases. (a) Ne-He, 700 torr, E = 11.2 kV/cm. (b) Ar, 310 torr, E = 13.4 kV/cm. (c) Ar + methane (7%), 310 torr, E = 13.4 kV/cm. (d) Ar + methane (3.5%), 310 torr, E = 11.4 kV/cm, parallel (top) and perpendicular (bottom) to E. (e) same as (d) except 1.75% methane. (f) Xe, 210 torr, E = 11.4 kV/cm, parallel (top) and perpendicular (bottom) to E. Length of the photographic image is 15 cm.

Fig. 13. The fragmentation of ^{12}C at 420 MeV into two heavy ions, with Ar-methane volume gas.

Fig. 7. Interaction of ^{12}C + Ne at 35 MeV/nucleon. Beam enters from the left.

Fig. 8. High voltage pulse profile monitored at the chamber. Record consists of approximately 250 consecutive Marx firings.

Fig. 9. Particle identification spectrum produced by a downstream Si(Li) ΔE-E telescope, for the reactions of ^{16}O + CsI at 16.5 MeV/nucleon. The spectrum was recreated in software, according to the scheme of Fig. 6(b).

Fig. 10. Typical events for ^{16}O induced reactions with mylar. Beam enters from the right; mid-target energy is approximately 16.5 MeV/nucleon. Arrow to the left of each photograph indicates the trigger particle and its identity according to the gate number.

Fig. 11. Associated multiplicity distributions as a function of ejectile and angle for ^{16}O + CsI at 16.5 MeV/nucleon. (Preliminary data.)

Fig. 12. Tracks of ^{90}Sr β^- in the 88-inch cyclotron streamer chamber with various gases. (a) Ne-He, 700 torr, E = 11.2 kV/cm. (b) Ar, 310 torr, E = 13.4 kV/cm. (c) Ar + methane (7%), 310 torr, E = 13.4 kV/cm. (d) Ar + methane (3.5%), 310 torr, E = 11.4 kV/cm, parallel (top) and perpendicular (bottom) to E. (e) same as (d) except 1.75% methane. (f) Xe, 210 torr, E = 11.4 kV/cm, parallel (top) and perpendicular (bottom) to E. Length of the photographic image is 15 cm.

Fig. 13. The fragmentation of ^{12}C at 420 MeV into two heavy ions, with Ar-methane volume gas.

Fig. 7. Interaction of ^{12}C + Ne at 35 MeV/nucleon. Beam enters from the left.

Fig. 8. High voltage pulse profile monitored at the chamber. Record consists of approximately 250 consecutive Marx firings.

Fig. 9. Particle identification spectrum produced by a downstream Si(Li) ΔE-E telescope, for the reactions of ^{16}O + CsI at 16.5 MeV/nucleon. The spectrum was recreated in software, according to the scheme of Fig. 6(b).

Fig. 10. Typical events for ^{16}O induced reactions with mylar. Beam enters from the right; mid-target energy is approximately 16.5 MeV/nucleon. Arrow to the left of each photograph indicates the trigger particle and its identity according to the gate number.

Fig. 11. Associated multiplicity distributions as a function of ejectile and angle for ^{16}O + CsI at 16.5 MeV/nucleon. (Preliminary data.)

Fig. 12. Tracks of ^{90}Sr β^- in the 88-inch cyclotron streamer chamber with various gases. (a) Ne-He, 700 torr, E = 11.2 kV/cm. (b) Ar, 310 torr, E = 13.4 kV/cm. (c) Ar + methane (7%), 310 torr, E = 13.4 kV/cm. (d) Ar + methane (3.5%), 310 torr, E = 11.4 kV/cm, parallel (top) and perpendicular (bottom) to E. (e) same as (d) except 1.75% methane. (f) Xe, 210 torr, E = 11.4 kV/cm, parallel (top) and perpendicular (bottom) to E. Length of the photographic image is 15 cm.

Fig. 13. The fragmentation of ^{12}C at 420 MeV into two heavy ions, with Ar-methane volume gas.

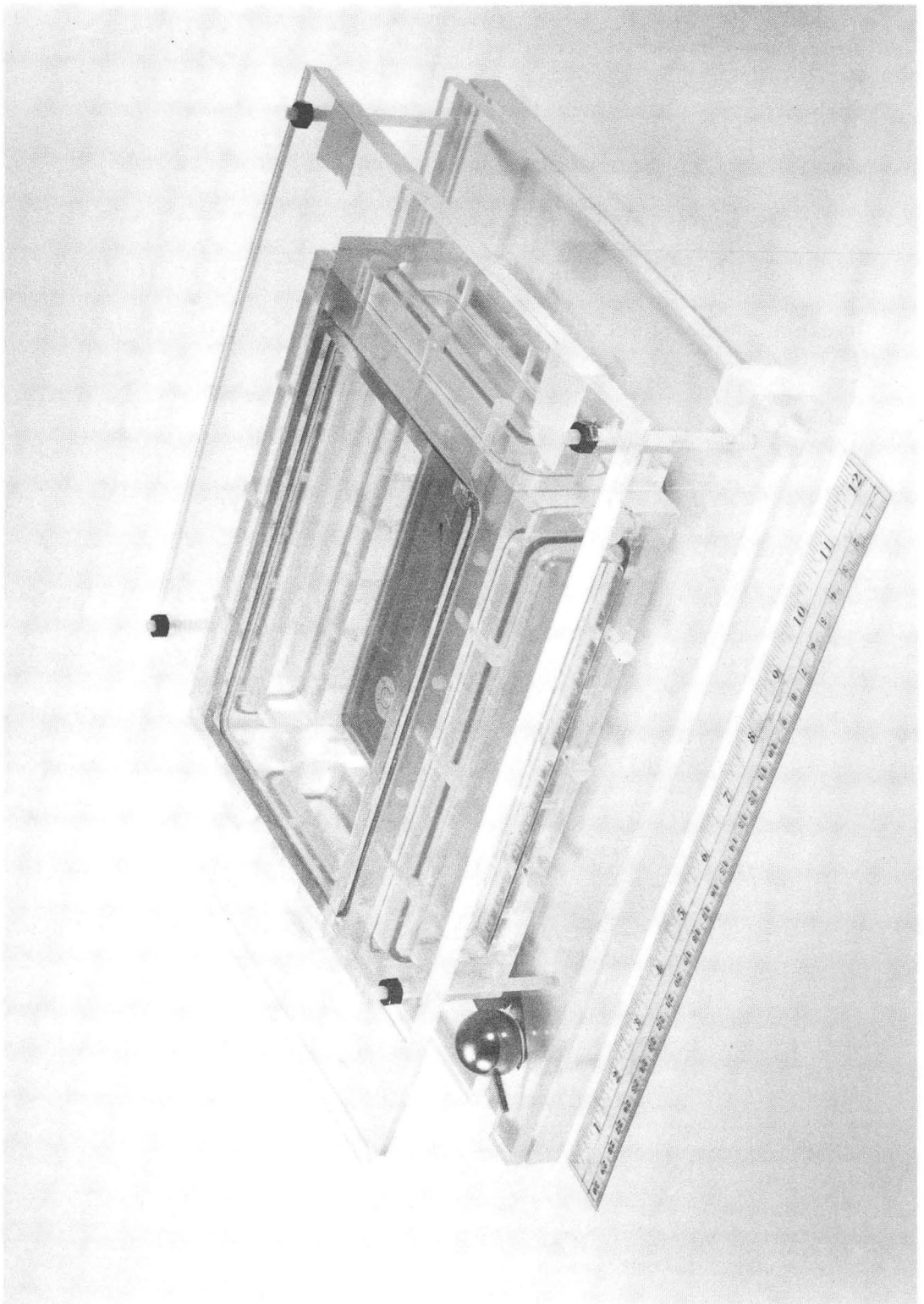

XBB 795-7440

Fig. 1

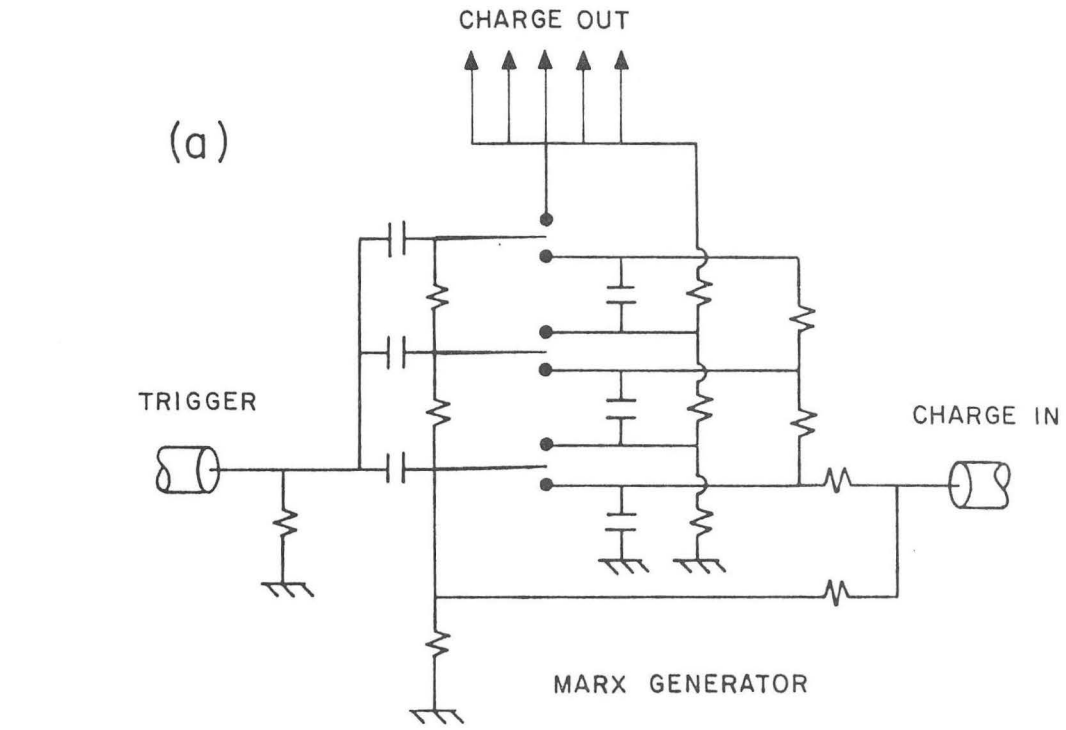
CHARGE OUT
(a)
TRIGGER
CHARGE IN
MARX GENERATOR

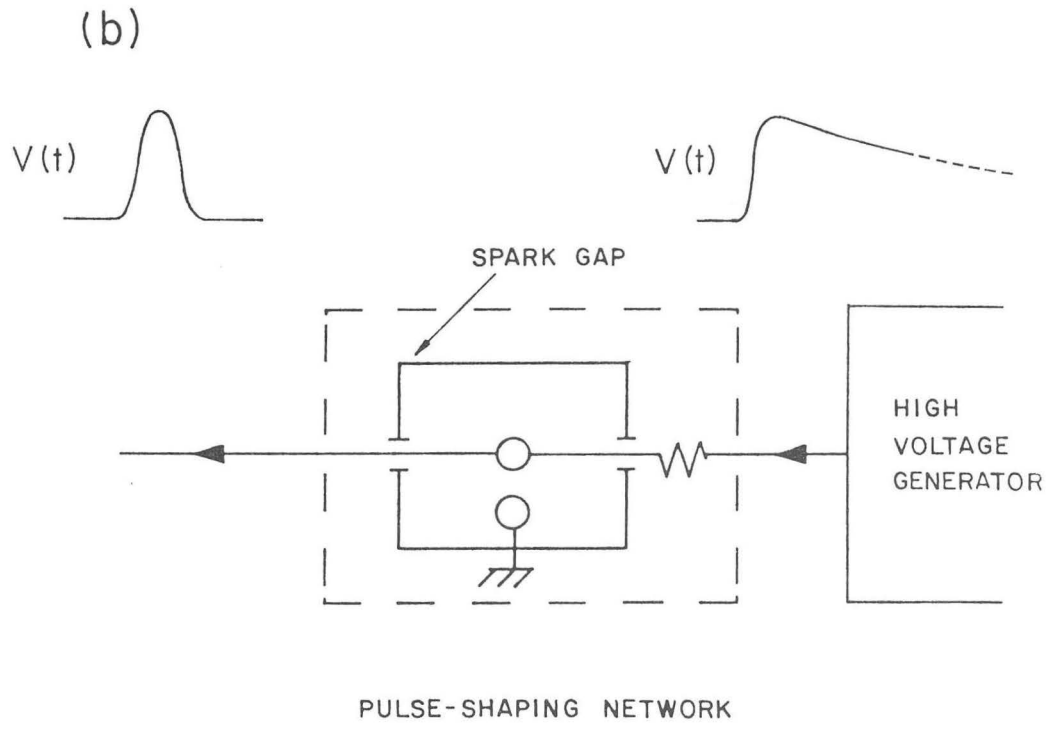
(b)
V(t)
V(t)
SPARK GAP
HIGH
VOLTAGE
GENERATOR
PULSE-SHAPING NETWORK

XBL 812-272

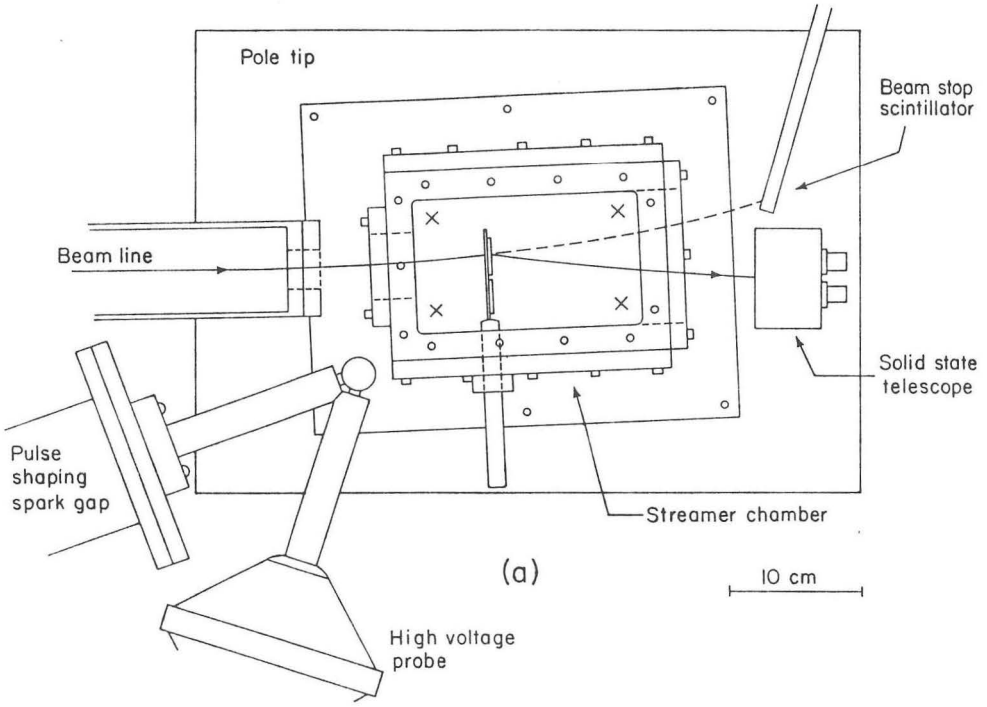
Pole tip
Beam stop scintillator
Beam line
Solid state telescope
Pulse shaping spark gap
Streamer chamber
(a)
10 cm
High voltage probe

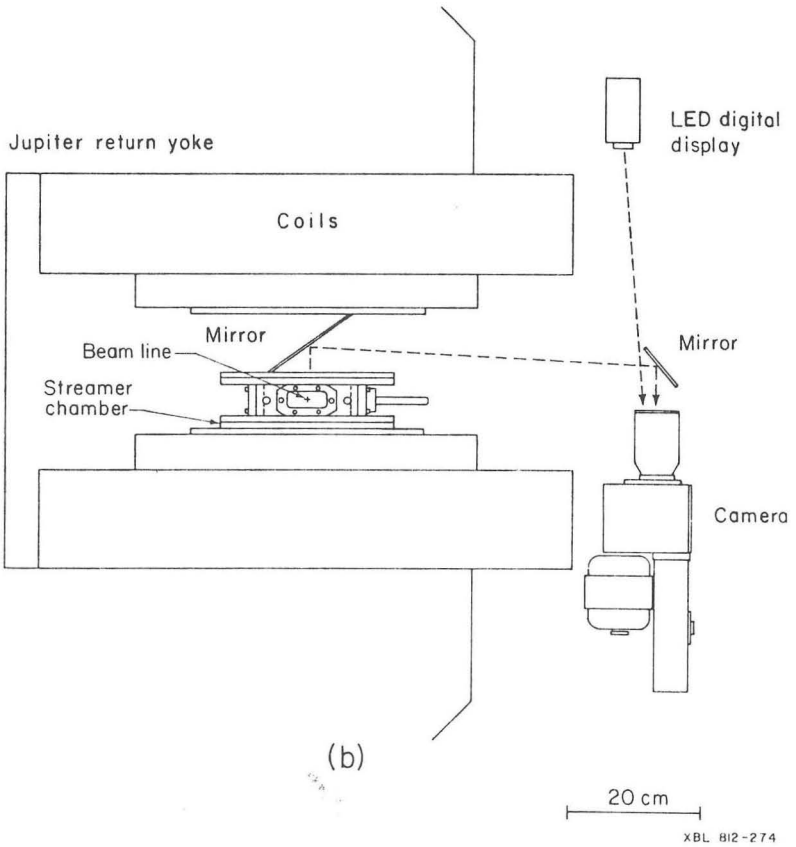
Jupiter return yoke
LED digital display
Coils
Mirror
Beam line
Mirror
Streamer chamber
Camera
(b)
20 cm
XBL 812-274

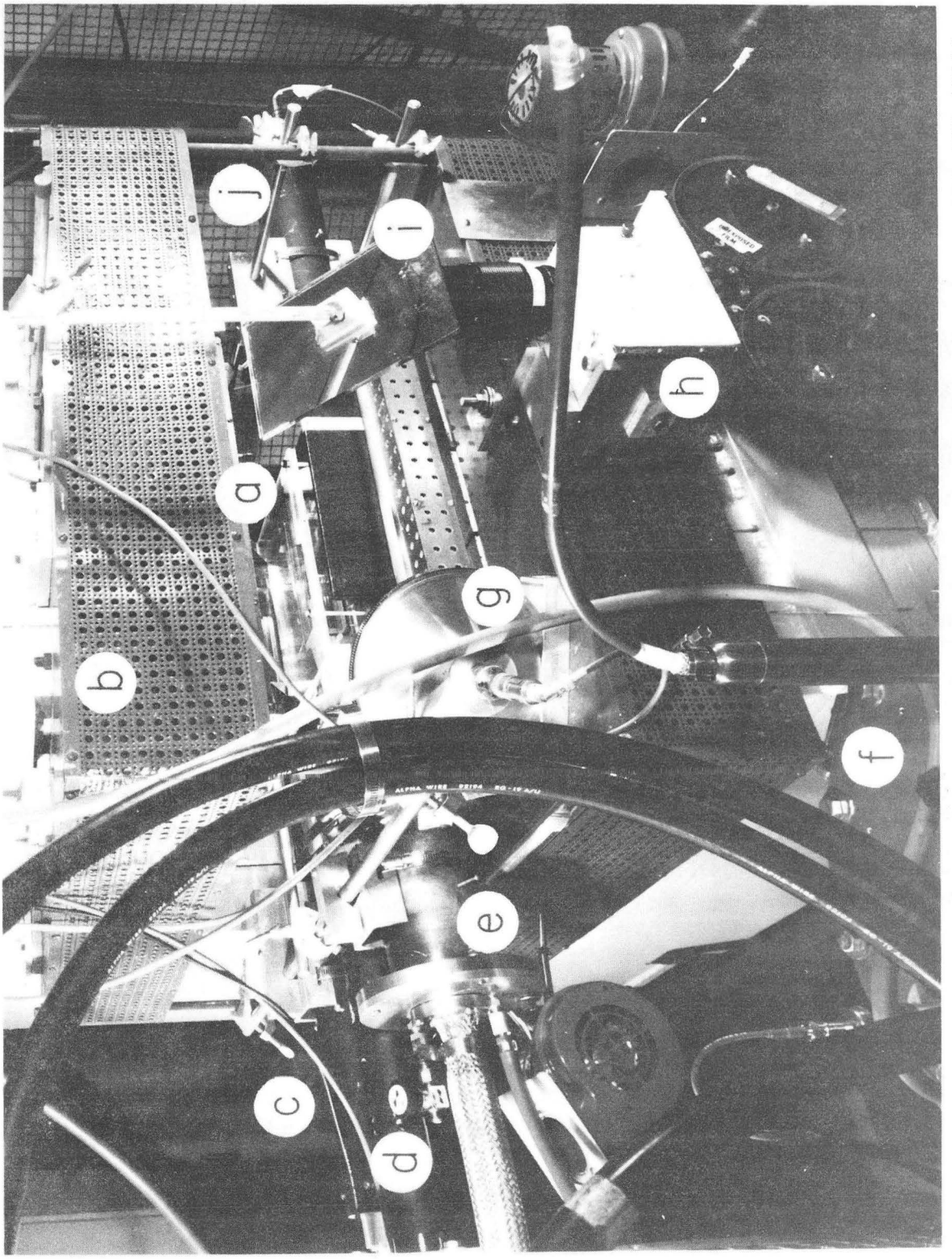

XBB 794-4911A

Fig. 4

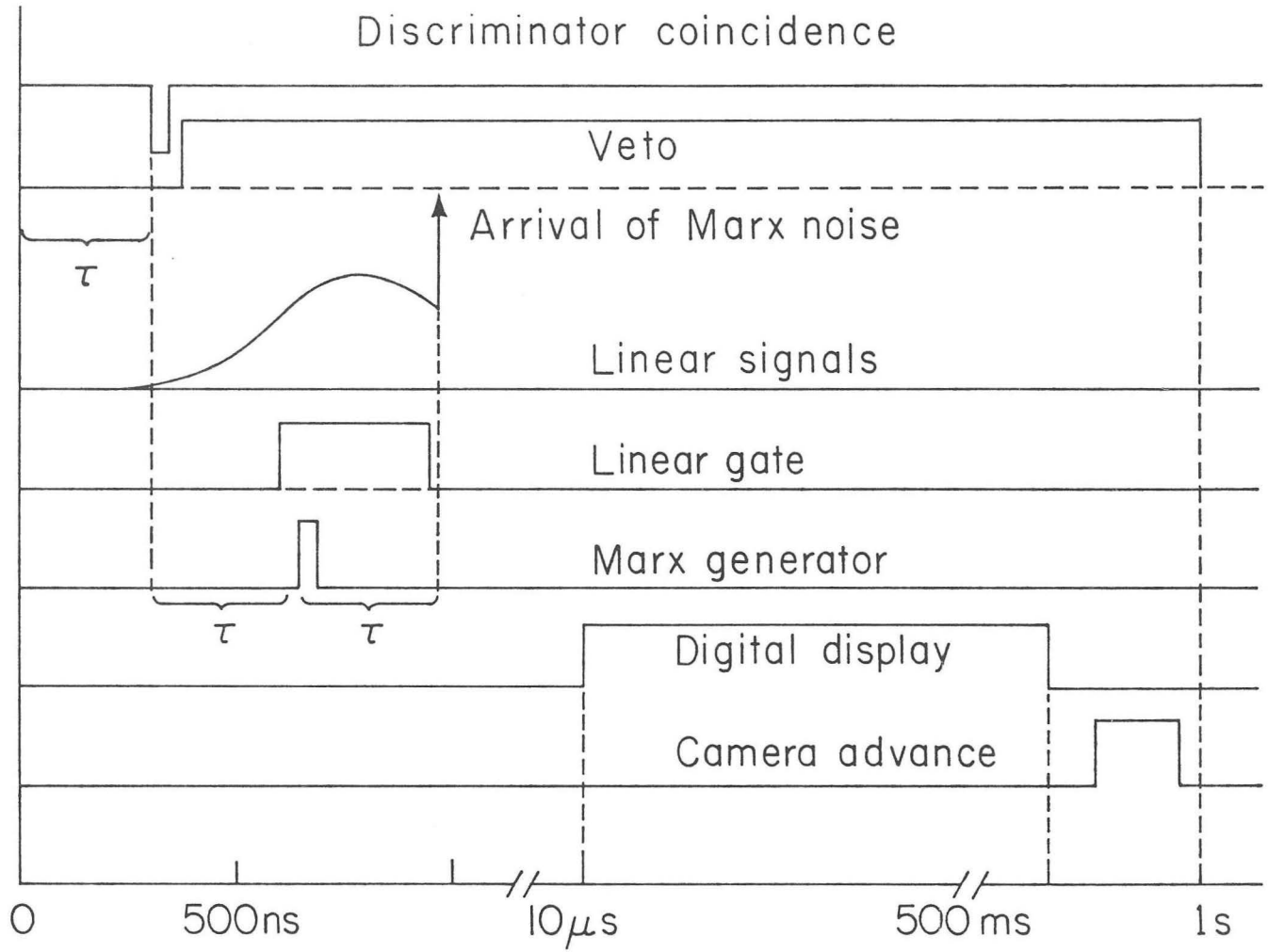

TIME AFTER EVENT

XBL-812-281

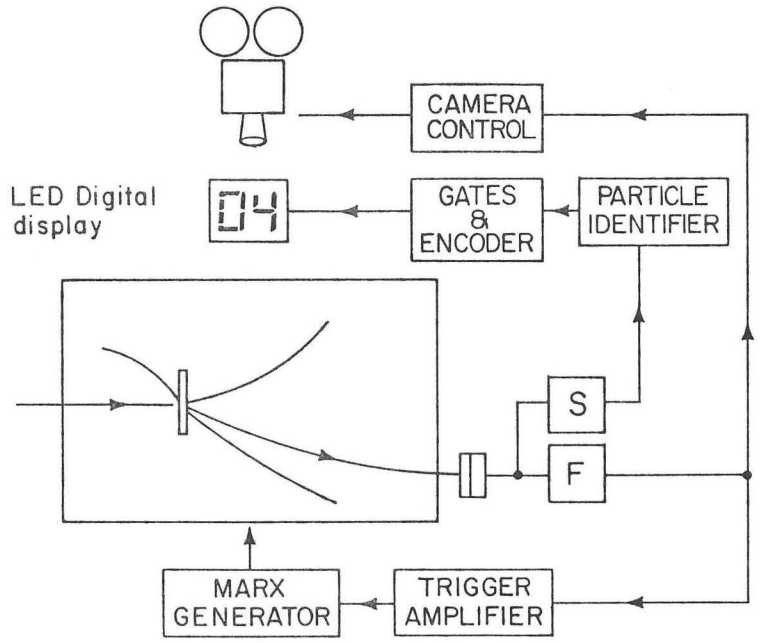

(a)

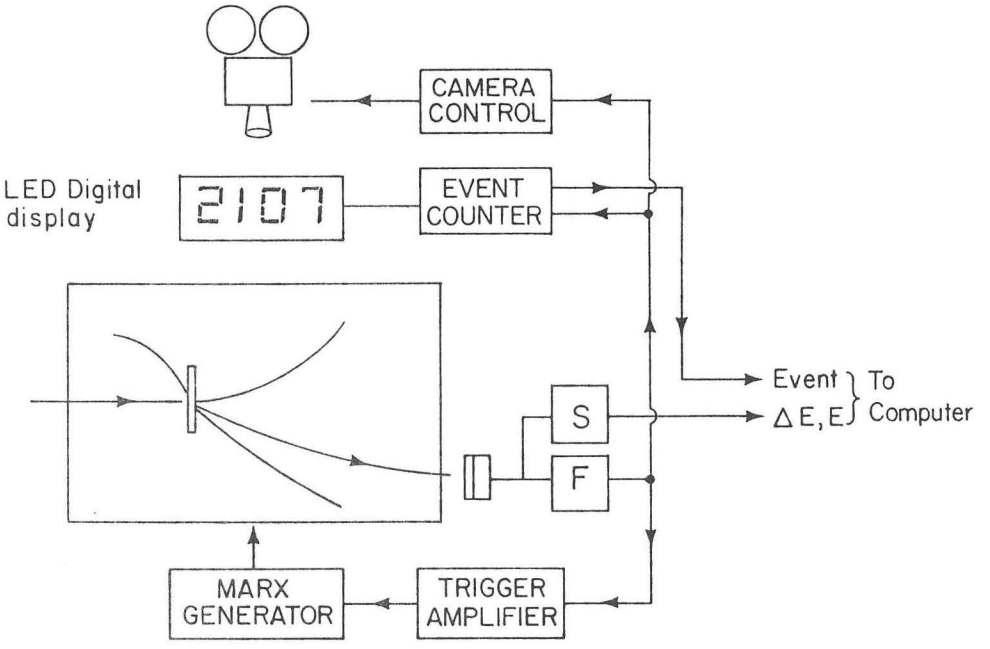

(b)

XBL 812-282

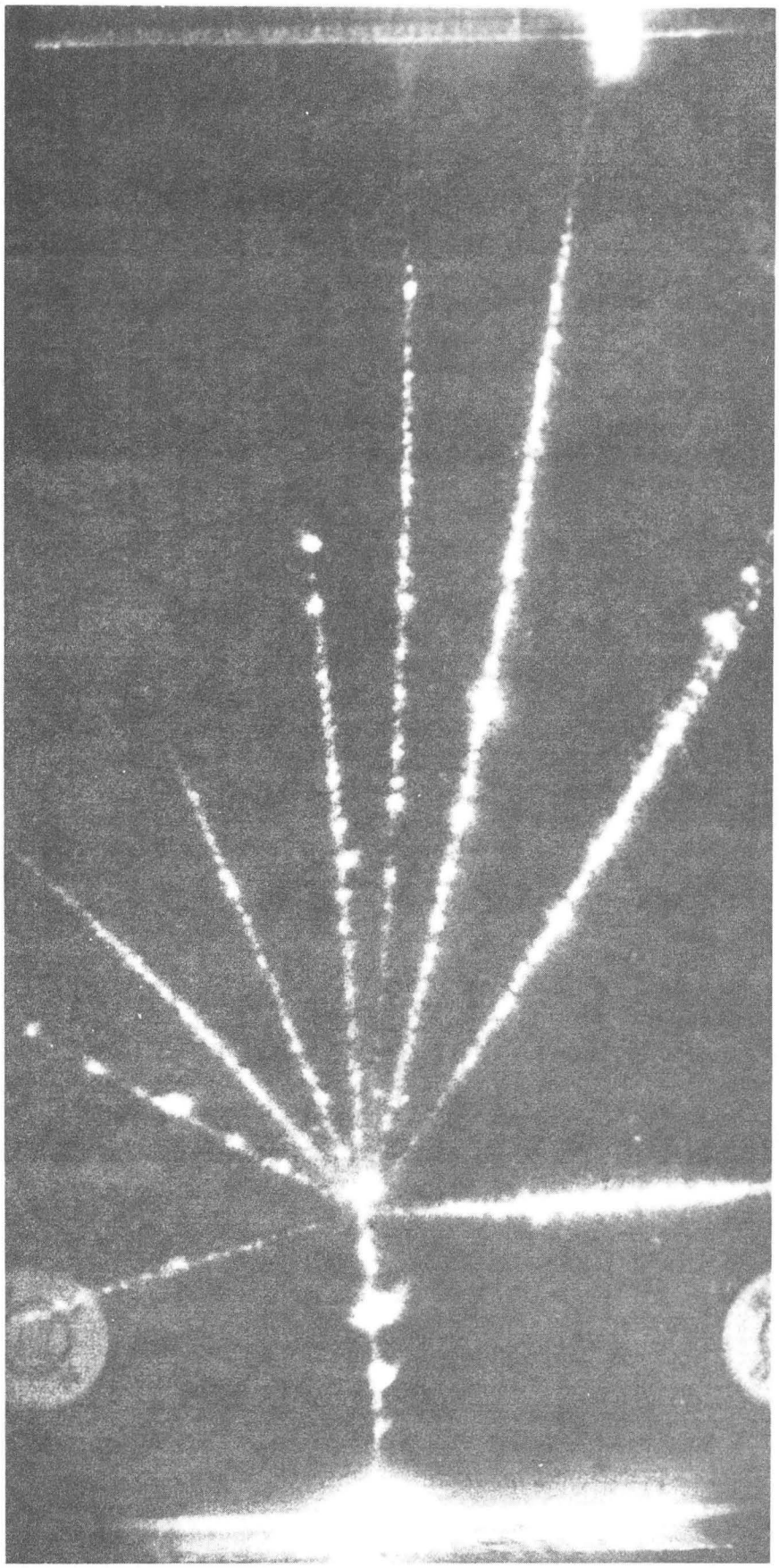

XBB 798-11198

Fig. 7

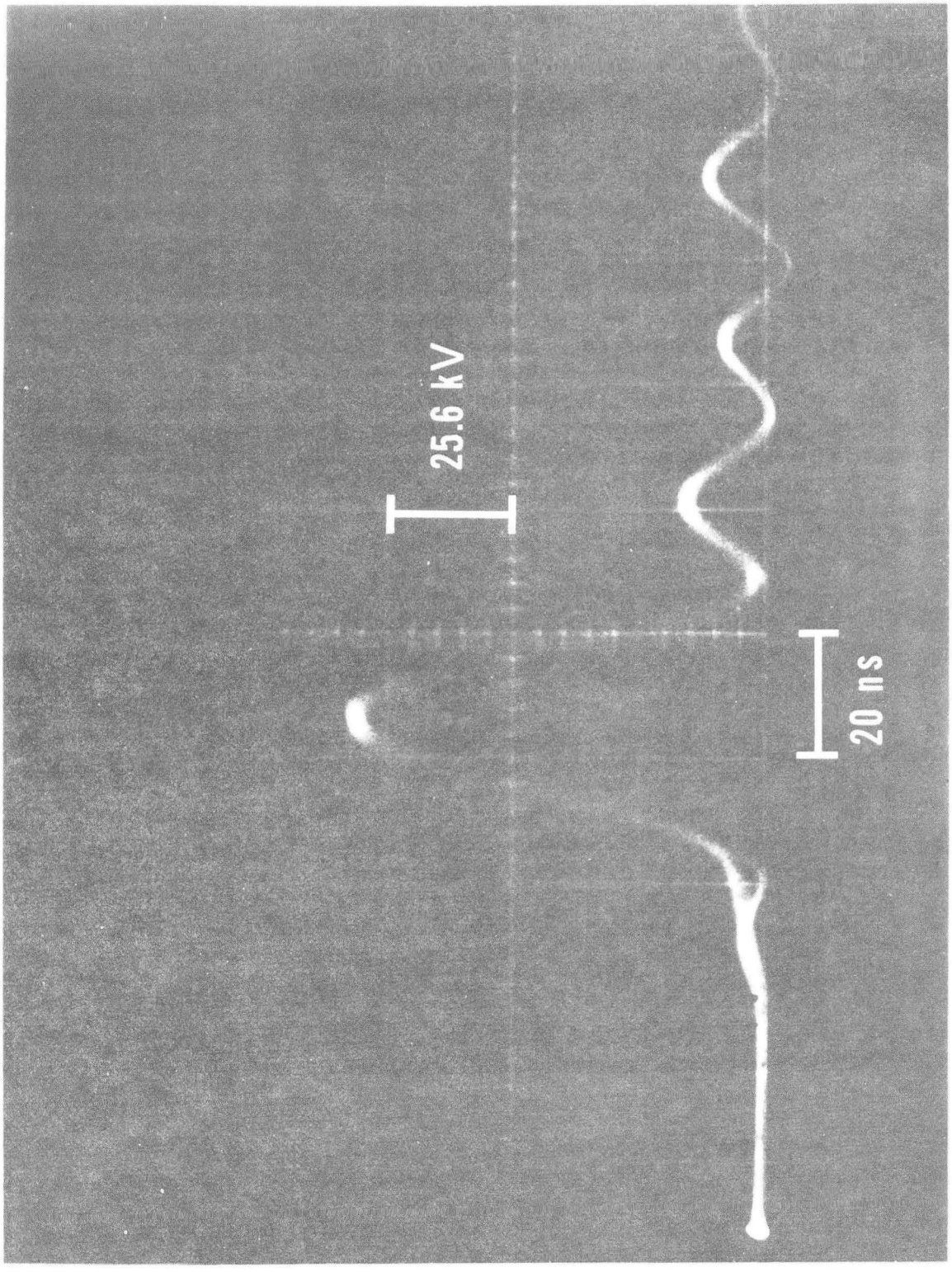

Fig. 8

XBB 812-2022

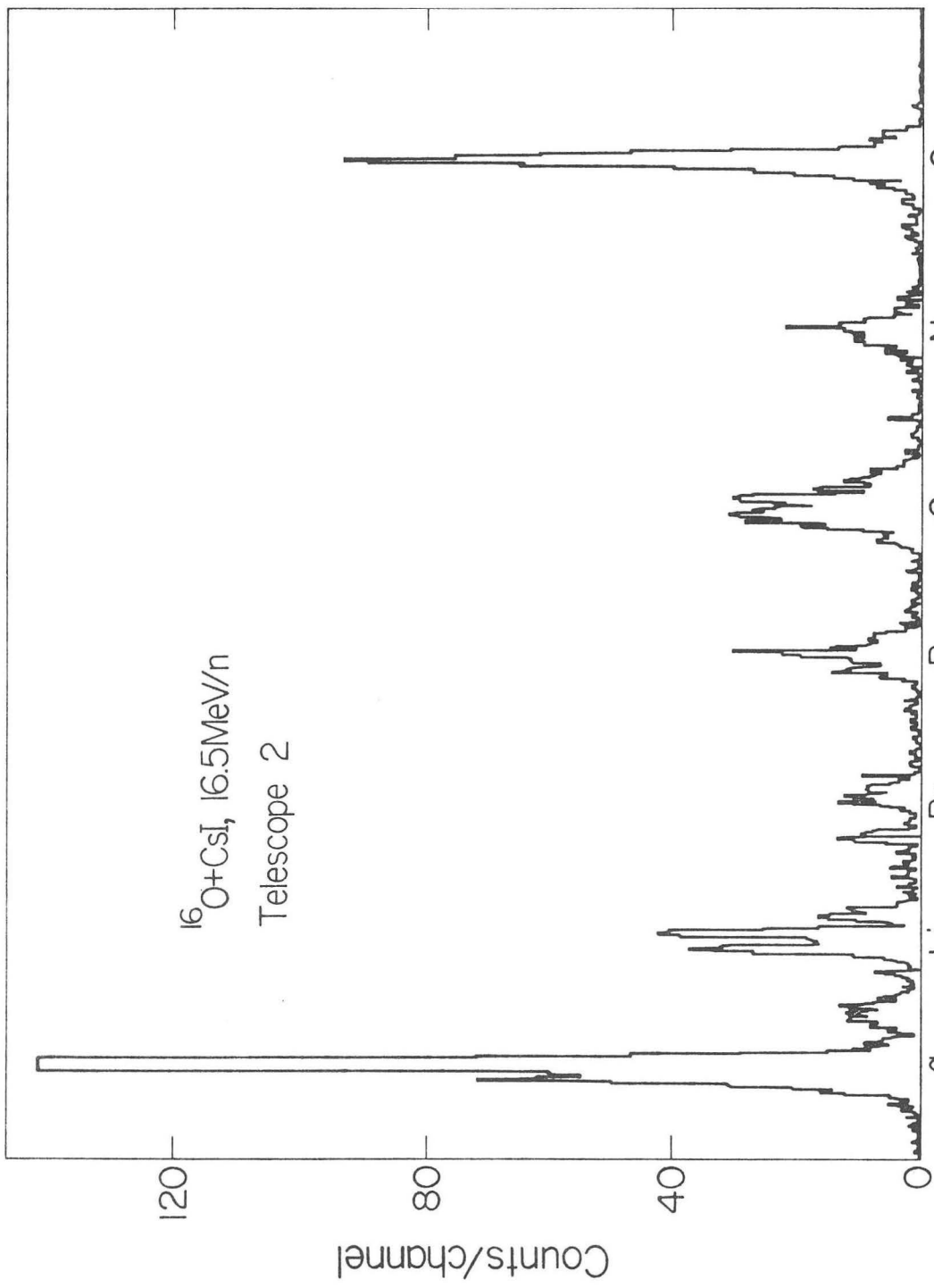
^{16}O+CsI, 16.5MeV/n
Telescope 2
Counts/channel
120
80
40
0
α
Li
Be
B
C
N
O
Particle identification

XBL 819-1316

(a)

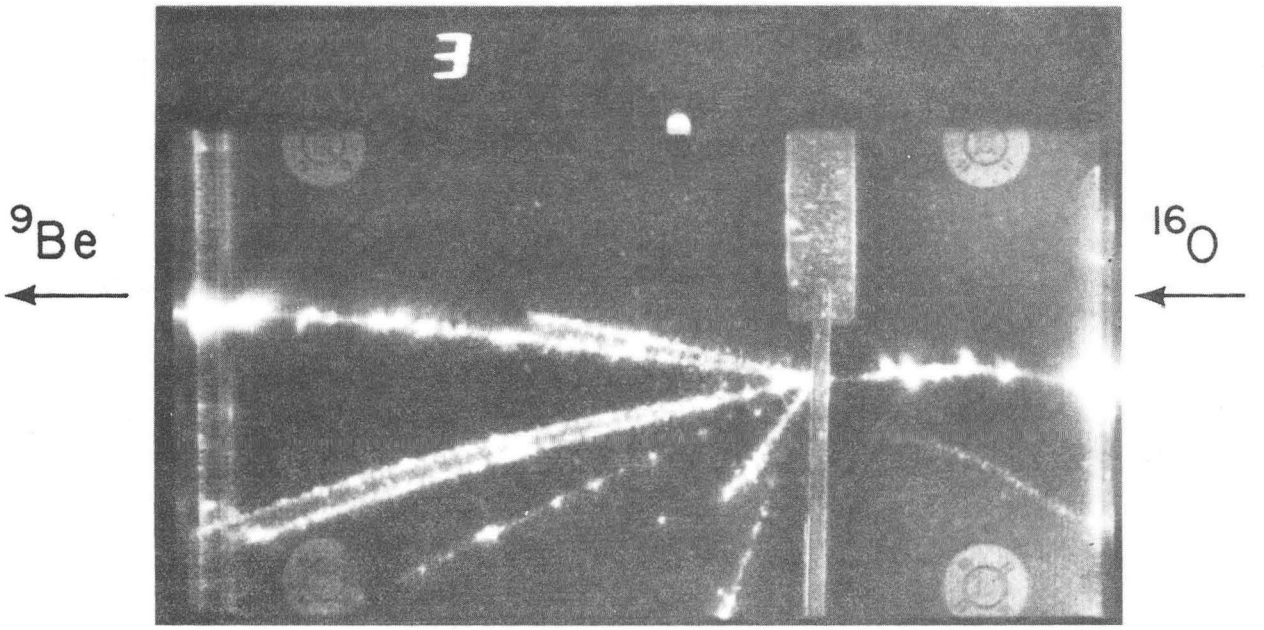

(b)

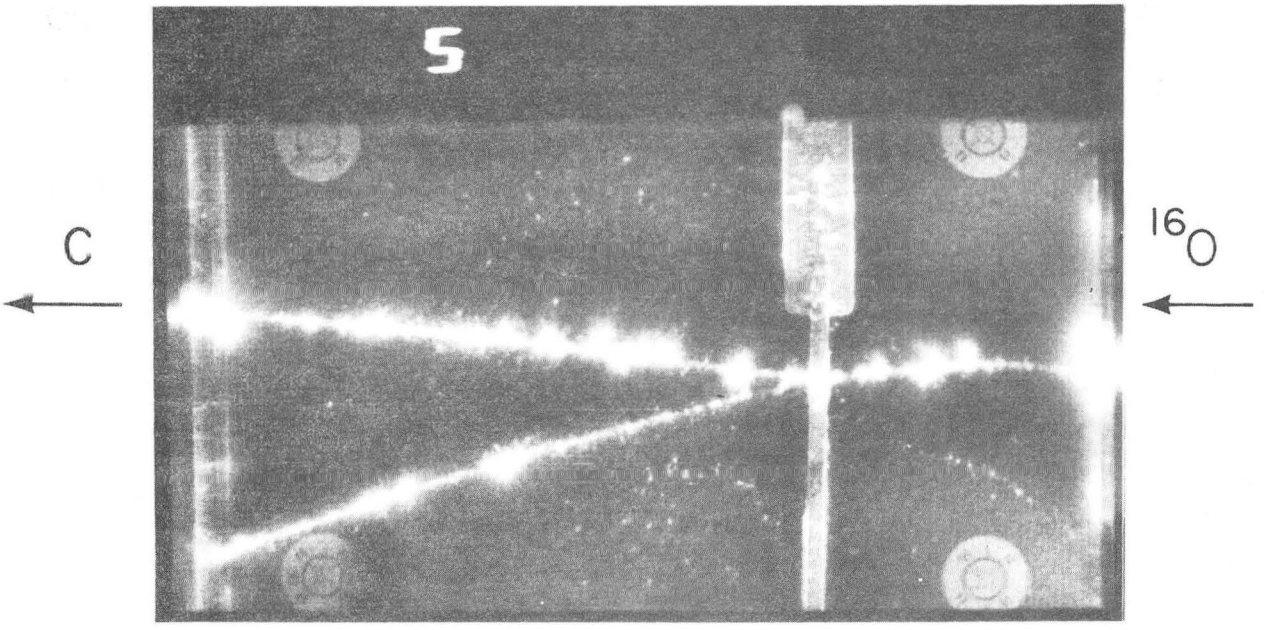

Fig. 10

XBB 812-2023

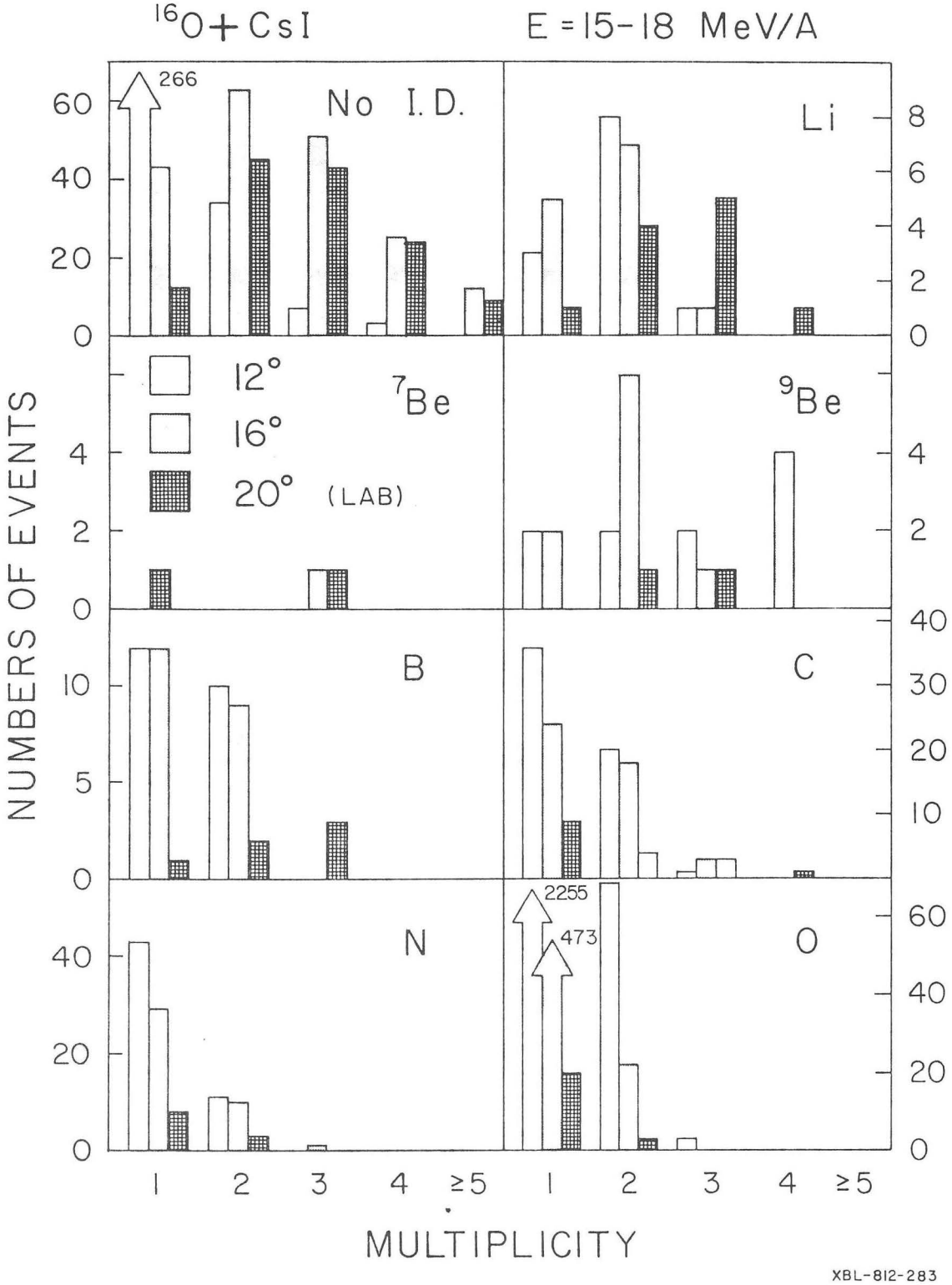
$^{16}O + CsI$
E = 15-18 MeV/A
No I.D.
Li
^{7}Be
^{9}Be
B
C
N
O
12°
16°
20° (LAB)
266
2255
473
NUMBERS OF EVENTS
MULTIPLICITY
1
2
3
4
≥5
XBL-812-283

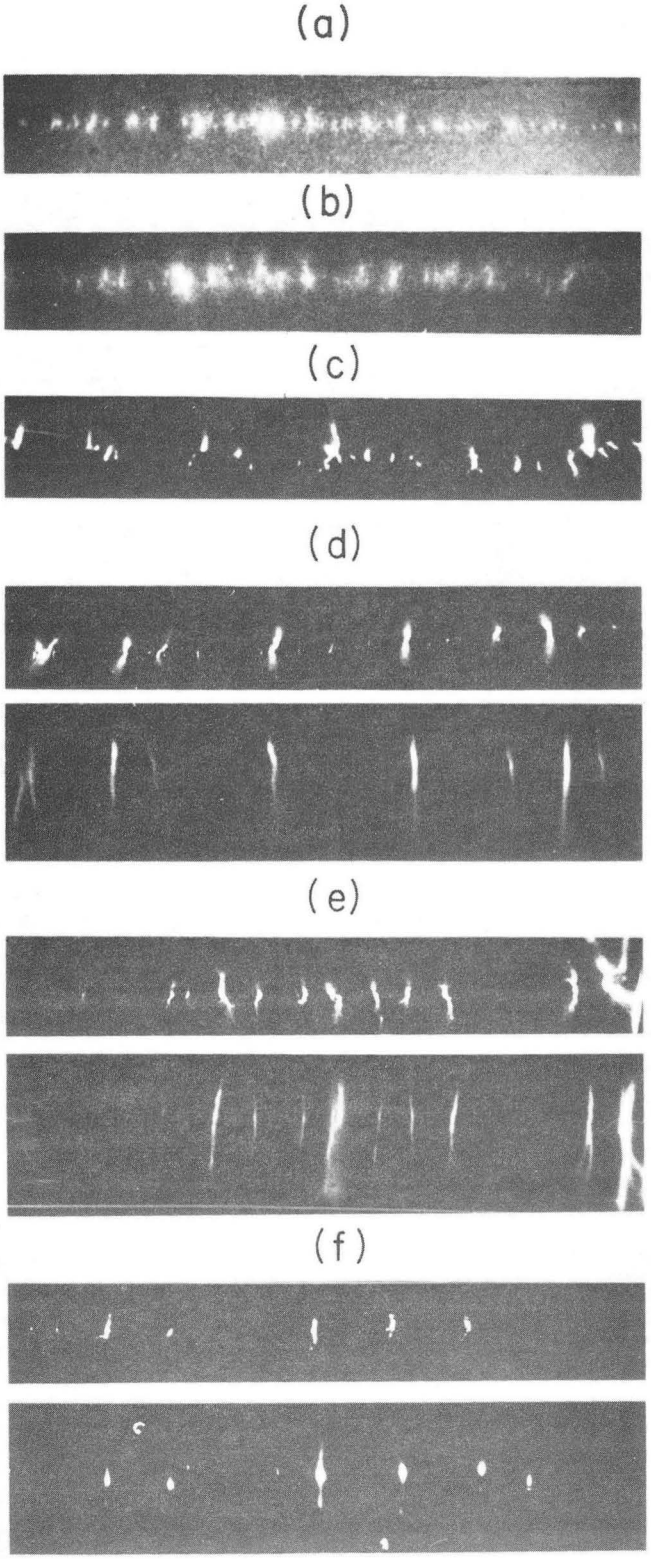

Fig. 12 XBB 790-13563

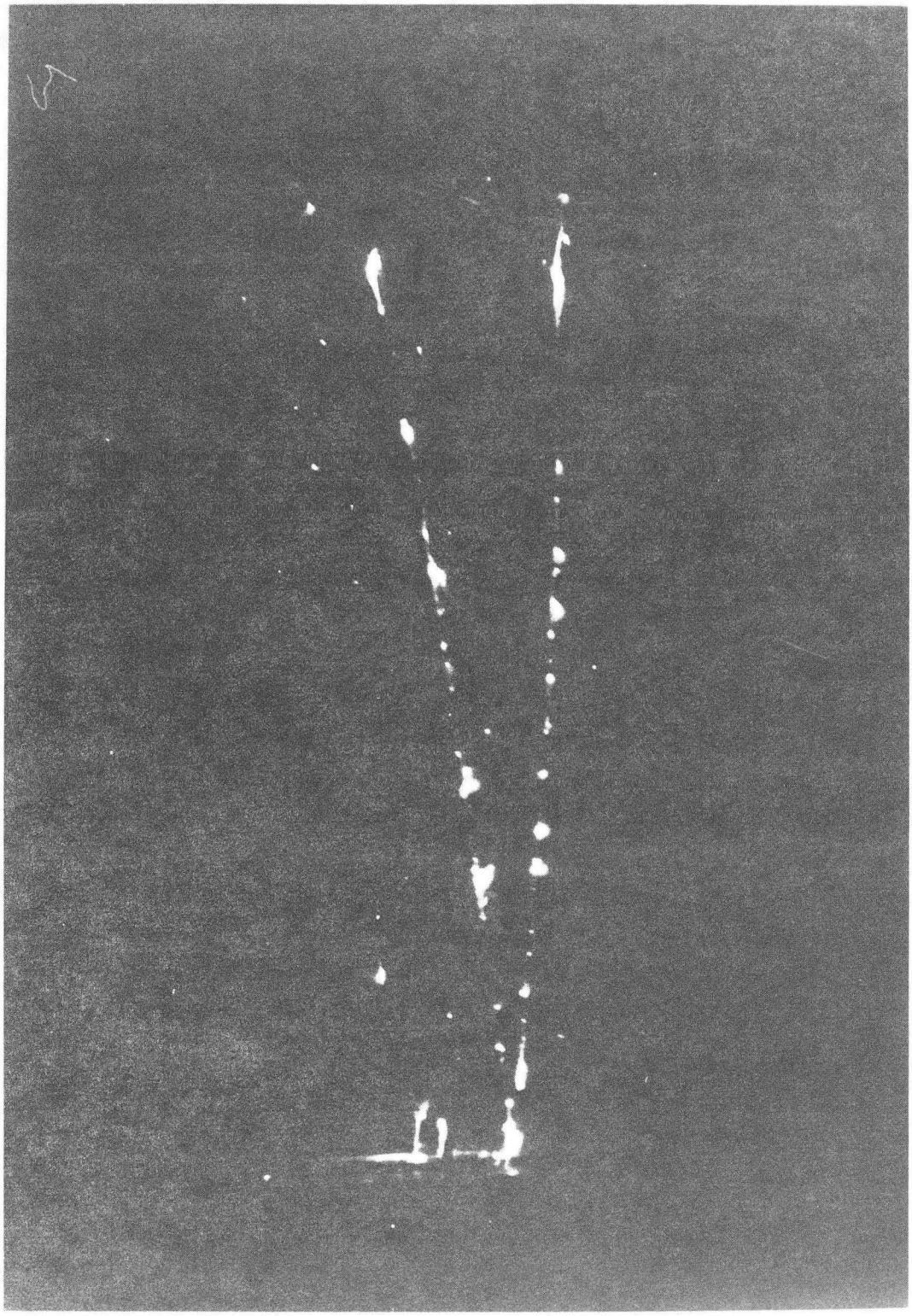

XBB 799-12806

Fig. 13

TECHNICAL INFORMATION DEPARTMENT
LAWRENCE BERKELEY LABORATORY
UNIVERSITY OF CALIFORNIA
BERKELEY, CALIFORNIA 94720